Marine Chemistry 233 (2021) 103983

Contents lists available at ScienceDirect

Marine Chemistry

journal homepage: www.elsevier.com/locate/marchem

Thermodynamic uptake of atmospheric CO_2 in the oligotrophic and semiarid São Francisco estuary (NE Brazil)

Gwenaël Abril [a,b,*], Bruno G. Libardoni [b], Nilva Brandini [b], Luiz C. Cotovicz Jr [c], Paulo R. P. Medeiros [d], Geórgenes H. Cavalcante [e,f], Bastiaan A. Knoppers [b]

[a] Laboratoire de Biologie des Organismes et Ecosystèmes Aquatiques (BOREA), Muséum National d'Histoire Naturelle, UMR 8067, CNRS, MNHN, IRD, SU, UCN, UA, Paris, France
[b] Programa de Geoquímica, Universidade Federal Fluminense, Niterói, RJ, Brazil
[c] Instituto de Ciências do Mar, Universidade Federal do Ceará, Fortaleza, Ceará, Brazil
[d] Instituto de Geografia Desenvolvimento e Meio Ambiente, Universidade Federal de Alagoas, Maceio, AL, Brazil
[e] Instituto de Ciências Atmosféricas, Universidade Federal de Alagoas, Maceio, AL, Brazil
[f] Department of Biology, Chemistry and Environmental Sciences, College of Arts and Sciences, American University of Sharjah, Sharjah, United Arab Emirates

A B S T R A C T

Estuarine carbonate chemistry predicts that thermodynamic equilibration during the mixing of freshwater with seawater will generate a carbon dioxide (CO_2) sink in the case of warm and poorly buffered tropical rivers. The São Francisco River estuary has historically become oligotrophic after the construction of a series of hydroelectric dams in its watershed, where organic matter and nutrients are retained. During two cruises in late winter (Aug. 2014) and early summer (Nov. 2015), dissolved inorganic carbon (DIC) and total alkalinity (TA) were found to increase linearly with salinity in the main estuarine channel, where water mixing required half a day, and showed nearly conservative behaviour. In the main channel, the water partial pressure of CO_2 (pCO_2) recorded at a 1-min frequency followed an asymmetric bell-shaped trend versus salinity, similar to the curve predicted by the thermodynamic conservative mixing of freshwater DIC and TA with seawater DIC and TA. The low (0–3) salinity region was always a source of atmospheric CO_2, where despite low chlorophyll concentrations, a pCO_2 diurnal change of approximately 60 ppmv suggested the occurrence of photosynthesis in summer. At salinities above 3, undersaturated pCO_2 values (down to 225 ppmv in winter and neap tides) and invasion of atmospheric CO_2 of 0.38–1.70 mmol m^{-1} h^{-1} occurred because of the predominating thermodynamics during estuarine mixing. In winter and neap tides, the higher river discharge, intense estuarine mixing, lower temperatures and limited tidal pumping resulted in observed pCO_2 differences from the theoretical conservative pCO_2 by less than 3 ppmv at salinities >3. Conversely, in summer and spring tides, the recorded pCO_2 values were on average + 43 ± 35 ppmv above the conservative mixing curve, when tidal pumping, CO_2 invasion and surface heating were more significant in the mixing zone but not sufficient to offset the thermodynamic uptake of atmospheric CO_2. By combining carbonate chemistry with estuarine mixing modelling and gas exchange calculations, we estimate that heating contributed to approximately 15% and gas exchange contributed to approximately 10% of the positive pCO_2 deviation from conservative mixing during summer. The remaining 75% of the deviation reached its maximum at ebb tides and within salinity ranges consistent with the occurrence of tidal pumping from marches and mangrove soils. Indeed, in the mangrove channel, water was supersaturated, with pCO_2 values of 976 ± 314 ppmv, while in the main channel, the highest positive pCO_2 deviations from conservative mixing (up to +100 ppmv for several hours) occurred at ebb tides. An important finding was that in São Francisco, the thermodynamic and biological processes compete with each other for CO_2 fluxes both at low salinities where evasion and autotrophy occur and at high salinities where invasion, heterotrophy and tidal pumping occur. Our study suggests that carbonate thermodynamics during mixing is a key process that has been overlooked in estuarine studies, although they can generate important air-water CO_2 exchange and significantly contribute to the carbon budget of estuaries and river plumes.

1. Introduction

The necessity of reducing uncertainties in global estimates of CO_2 sources and sinks on Earth has promoted research on the carbon cycle in estuarine and coastal ecosystems, particularly during the last three decades (Wollast, 1991; Smith and Hollibaugh, 1993; Frankignoulle et al., 1998; Cai, 2011; Borges and Abril, 2011; Bauer et al., 2013; Dinauer and Mucci, 2017; Maher et al., 2018). Despite their small surface areas, estuaries have been identified as a hotspot of CO_2 emissions, able to offset a large part of the CO_2 sink on the continental shelves (Chen and Borges, 2009). This conclusion was based on field observations in temperate and boreal regions, where estuaries have been recognized as CO_2 sources and heterotrophic ecosystems, with negative net ecosystem production (NEP) (Smith and Hollibaugh, 1993; Borges and Abril, 2011). Upper

* Corresponding author at: Laboratoire de Biologie des Organismes et Ecosystèmes Aquatiques (BOREA), Muséum National d'Histoire Naturelle, UMR 8067, CNRS, MNHN, IRD, SU, UCN, UA, Paris, France.
E-mail address: gwenael.abril@mnhn.fr (G. Abril).

https://doi.org/10.1016/j.marchem.2021.103983
Received 3 November 2020; Received in revised form 20 April 2021; Accepted 24 April 2021
Available online 15 May 2021

estuarine regions with generally well-mixed channels are almost always net heterotrophic, supersaturated in CO_2 and strong sources of CO_2 for the atmosphere (Frankignoulle et al., 1998; Borges et al., 2006; Sarma et al., 2012; Chen et al., 2012). In contrast, lower estuarine regions with high salinities, including large surfaces of river plumes at sea and coastal embayments, are sites of phytoplankton blooms and may have a net autotrophic metabolism (positive NEP) at least in the surface layer and behave as CO_2 sinks at minima seasonally (Körtzinger, 2003; Borges et al., 2006; Chen et al., 2012; Cai et al., 2013; Cotovicz Jr. et al., 2015; Lefèvre et al., 2017).

Global CO_2 emissions from estuaries suffer from large uncertainties due to spatial and temporal heterogeneity (Chen and Borges, 2009; Chen et al., 2012). In most studies, the relationship between NEP and CO_2 fluxes could not be established quantitatively because many processes other than community respiration and primary production can alter the partial pressure of CO_2 (pCO_2) and the direction and intensity of the air-sea CO_2 flux in estuaries (Borges, 2005). For instance, in eutrophic estuaries, nitrification can titrate TA to CO_2, contrary to carbonate dissolution, which can consume CO_2 and generate TA (Frankignoulle et al., 1996; Abril and Frankignoulle, 2001; Abril et al., 2003; Cotovicz Jr. et al., 2021). Some dissolved CO_2 transported laterally from freshwaters, or tidal marshes and mangroves is ventilated in river-dominated and/or macrotidal estuaries (Abril et al., 2000; Neubauer and Anderson, 2003; Borges et al., 2003, 2006; Cai, 2011). In general, the advection of surface or subsurface waters enriched in DIC and/or biodegradable organic carbon (OC), as well as the presence of vegetation at the land-water interface, complicates the calculation of NEP and its relationship with CO_2 fluxes (Borges, 2005; Cai, 2011; Borges and Abril, 2011; Santos et al., 2018; Maher et al., 2018).

In estuaries, water pCO_2 is also strongly modified by the displacement of the acid-base equilibria of the carbonate system during the mixing of freshwater with seawater. As a consequence, the concentrations of bicarbonate (HCO_3^-) and carbonate (CO_3^{2-}) ions, as well as pCO_2 in a mixture of two water types with different salinities and temperatures, are very different from the arithmetic mean of these parameters in the two water types. In their pioneering theoretical work, Whitfield and Turner (1986) applied newly published carbonate dissociation and gas solubility constants to calculate the theoretical distribution of pCO_2 along the salinity gradient induced by the conservative mixing of DIC and TA from freshwater and marine end-members. These authors showed that "*the mixing of river water and seawater […] tends to produce significant disequilibrium between the estuary and the atmosphere which may manifest itself as a deficit or as an excess of carbon dioxide, depending on the pH and alkalinity of the river water.*" However, in recent years, studies rarely considered in detail carbonate thermodynamic during mixing as a potential driver of estuarine CO_2 fluxes, although this thermodynamic can generate some atmospheric CO_2 release or uptake additional to NEP (Cai et al., 2013; Lefèvre et al., 2017; Delaigue et al., 2020; Cotovicz Jr. et al., 2020). Most studies have focused on the correlation between the biological components of NEP and CO_2 fluxes (Borges and Abril, 2011) and lateral C fluxes induced by tidal inundation and pumping (Cai, 2011; Maher et al., 2013, 2018). In the Amazon plume, a large part of the CO_2 sink at salinities higher than 17 could be attributed to thermodynamics, but unfortunately, no pCO_2 field data are available at salinities lower than 17 (Körtzinger, 2003; Cai et al., 2013; Lefèvre et al., 2017). Recently, Cotovicz Jr. et al. (2020) reported a CO_2 sink in the estuarine delta of the Paraiba do Sul River induced by a combination of carbonate thermodynamics, ecosystem metabolism and temperature effects. Although it is essential in the open ocean, the role of surface water heating or cooling on CO_2 fluxes is poorly documented in estuarine waters. In tropical and subtropical coastal systems, surface heating and evaporation can significantly impact CO_2 water-air fluxes (Yao and Hu, 2017; Cotovicz Jr. et al., 2020; Yao et al., 2020).

In the present study, we report high-resolution data of the carbonate system in a tropical, oligotrophic estuary with a short mixing time, where thermodynamics alone explains a large part of the well-defined pCO_2 distribution. Owing to warm temperatures and low TA at the river end-member, the São Francisco estuary presents conditions that theoretically generate CO_2 invasion during estuarine mixing, even when supersaturation prevails in the river, a case similar to large tropical rivers such as the Amazon and the Congo (Cai et al., 2013). The oligotrophic character of the estuary and the short mixing time cause chemical and physical processes to predominate over biological processes. The estuary is also connected to a small mangrove forest that may export dissolved carbon to waters (Maher et al., 2013) and is subjected to important heating due to summer semiarid evaporative conditions.

2. Material and methods

2.1. Study area

The São Francisco River (Fig. 1) drains an area of 634,000 km^2 in Brazil that includes Pleistocene-Holocene plains (Dominguez, 1996). Precambrian rocks of the Brazilian shield dominate the geology of the basin, and the climate varies from tropical humid in the upper and lower regions to semiarid in the middle region (Bernardes, 1951). The river course was progressively intensively modified between the 1950s and 1990s by the construction of five hydroelectric reservoirs, which had strong impacts on the estuary. Decreased precipitation combined with increased evaporation due to the presence of dams in the watershed has reduced the average annual freshwater discharge from approximately 2895 $m^3\ s^{-1}$ (1961–1990) to approximately 1800 $m^3\ s^{-1}$ (after Xingó Dam) in 1995 and to less than 1000 $m^3\ s^{-1}$ during the last decade (Bernardes et al., 2012; Cavalcante et al., 2017; de Jong et al., 2018). Floods that strongly influenced the estuarine morphology were suppressed, and most of the riverine suspended sediments, nitrogen, phosphorus and silica were retained in reservoirs, turning the estuary oligotrophic, with chlorophyll concentrations (Chl *a*) lower than 3 μg L^{-1} in more than 95% of the samples from recent years (Medeiros et al., 2011, 2018; Melo et al., 2020; Melo-Magalhães et al., 2015). Today, the estuarine morphology consists of a stratified, salt-wedge type, main channel, separated from the sea by a shallow area of submerged dynamic sandy banks, and a secondary channel in the south, surrounded by mangroves that have been partly deforested for shrimp farming. Water depth in the main channel was on average 3 m, with a maximum of 12 m and very shallow depth at the mouth, where sandy banks separate the estuary from the shelf. Strong saline stratification occurs in the main channel, and tidal movements generate large variations in surface water salinity and extension of the plume on the shelf (Cavalcante et al., 2020). The residence time of freshwater in the inner estuary with a surface area of 19 km^2 is approximately half a day (Cavalcante et al., 2017). Approximately 5% of the freshwater transits through the secondary channel and ends up in a shallow coastal lagoon parallel to the coast and connected to the sea at high tide through several narrow canals (Fig. 1).

2.2. Fieldwork, chemical analyses and calculations

Sampling occurred in late winter on the 5th-8th of August 2014 and in early summer on the 11th-14th of November 2015, when river discharges were 1220 and 950 $m^3\ s^{-1}$, respectively, and the tidal ranges were 1.2 m (end of neap tides) and 1.8 m (spring tides). Detailed descriptions of all methods for in situ measurements, discrete water sampling and preservation can be found in Cotovicz Jr. et al. (2015) and Cotovicz Jr. et al. (2020). Fieldwork consisted of measuring pCO2, salinity and temperature every minute and sampling surface water from freshwater to coastal waters (salinity >30) in both channels. Discrete samples were taken along the salinity gradient in the two channels at approximately two salinity intervals, except in the salinity range of 10–25, where changes were too abrupt to allow sampling at regular salinity intervals. Three end-members could be sampled (Fig. 1): the centre of the river main channel, the mouth of the main channel (salinity ~30), and a shallow coastal lagoon at the outlet of the secondary

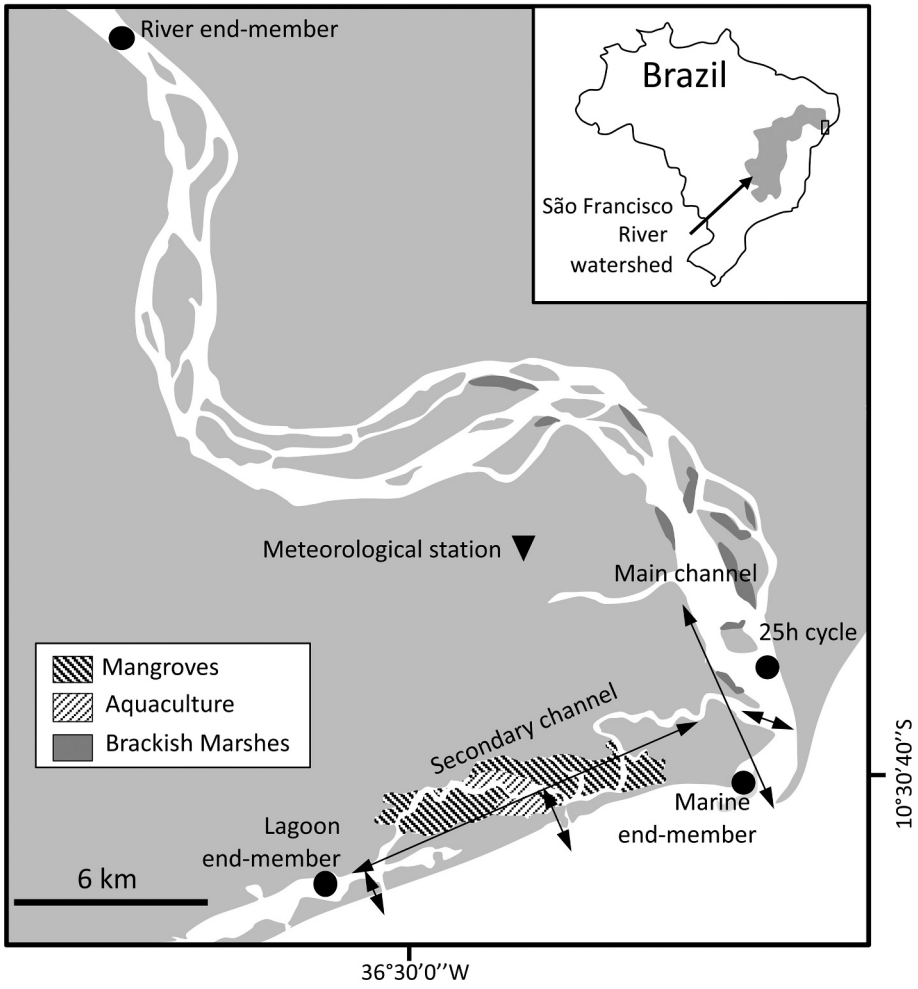

Fig. 1. Map of the São Francisco Estuary. Arrows show the regions of freshwater-estuarine water-seawater mixing and the approximate localisation of the salinity gradient in the main channel, sampled from the freshwater at the centre of the river until the seawater end-member (Salinity ~30–34) and in the shallow tidal lagoon end-member (Salinity ~34).

mangrove channel (salinity 30–34). On November 11–12, 2015, measurements were also performed for 25 h at an anchored station in the main channel, where salinity varied from 1.2 at low tide to 32.2 at high tide. Continuous measurements were performed during the vessel's travels or at the anchored station by pumping surface water at 8 L min^{-1} to a 1 L vial containing the sondes and a marble-type equilibrator (Frankignoulle et al., 2001). The marble equilibrator consisted of an acrylic tube filled with glass marbles where water flowed from the top and a closed air circuit with a flux of approximately 1 L min^{-1} flowing in the opposite direction from the bottom to the top. The air was dried with drierite and pumped to a nondispersive infrared (NDIR) gas analyser (LICOR© LI- 820). Before and after each sampling campaign, the NDIR was calibrated using gas standards with air pCO_2 values of 410, 1007 and 5035 ppmv (White Martins Certified Material, RJ, Brazil). Fresh soda lime was used to set the zero and the standard at 1007 ppmv to set the span. Air standards of 410 and 5035 ppmv were used to verify the linearity of the response. The accuracy of the pCO_2 measurements is estimated at ±5 ppmv. Water was continuously overflowing from the 1 L vial that hosted a YSI© Professional Plus multiparameter sonde that measured temperature, salinity, dissolved oxygen (DO), and a WTW© 3310 pH metre equipped with a Sentix 41 electrode. According to the National Institute of Standards and Technology (NIST), the pH metre was calibrated daily with a three-point standard (pH 4.01, pH 7.00 and pH 10.01). The precision of the pH measurements estimated after seven verifications against standards was approximately 0.01 NBS units. The salinity probe was calibrated before the cruise with IAPSO standard seawater and deionized water. DO was measured with a polarographic electrode calibrated every morning at 100% saturation in vapour-saturated air. Temperature values measured with the YSI© salinity probe differed from those measured with the WTW© pH metre by less than 0.1 °C. For continuous measurements performed during sailing, the ship speed was adapted according to the salinity changes. Discrete water samples were filtered on Whatman 0.7-μm GF/F filters (precombusted at 500 °C for 6 h), followed by determination of TA and Chl *a*. Total alkalinity (TA) was titrated with certified 0.1 N HCl on duplicate 50-mL filtered samples using the Gran function to determine the equivalent point. The accuracy was better than ±5 μmol kg^{-1}. The filters for analysis of Chl *a* were kept at −18 °C before analysis. Chl *a* was extracted from the filters with 90% acetone and quantified by spectrophotometry according to Strickland and Parsons (1972).

The concentration of DIC was calculated in discrete samples from the measured pCO_2 and TA with the CO2sys program (Pierrot et al., 2006) using the CO_2 solubility from Weiss (1974) and the dissociation constants of Mehrbach et al. (1973), refitted by Dickson and Millero (1987). One important precaution for the use of this set of constants is to check for the absence of organic alkalinity at significant concentrations compared to carbonate alkalinity, particularly in freshwaters (Cai et al., 1998; Hunt et al., 2011; Abril et al., 2015). To identify an eventual bias induced by the interference of organic alkalinity in DIC calculations, we used our pH measurements concomitant with TA measurements to

calculate pCO_2 (pH/TA) in our discrete samples. The pCO_2 values calculated from pH and TA and those measured directly with the equilibrator were fairly consistent (< ±10%), except in a small freshwater tributary on the left edge of the São Francisco River (north of Fig. 1 and Fig. S1) that drains a small wetland, where the calculated pCO_2 (pH/TA) was more than 4 times higher than the measured pCO_2 (Cotovicz Jr. et al., 2016). However, this tributary does not contribute significantly to river discharge, as confirmed by our conductivity monitoring at the confluence. Organic alkalinity does not appear to significantly interfere with the calculation of the carbonate system in the São Francisco main channel and mangrove channel.

In this work, we analysed and compared the distribution along the salinity gradient of four types of pCO_2: the pCO_2 observed in situ, referred to as O-pCO_2, the pCO_2 resulting from conservative mixing of river water with seawater, referred to as C-pCO_2, the pCO_2 normalized to temperature, referred to as T-pCO_2, and the pCO_2 resulting from conservative after being corrected for gas exchange, referred to as Ex-pCO_2. For each campaign, we established the equations of the conservative mixing lines for TA, DIC and temperature as a function of salinity using the values at the two end-members: the reference freshwater station at the centre of the main channel upstream and the most saline sample at the mouth downstream (Fig. 1). Then, the C-pCO_2 thermodynamic conservative mixing curves were calculated for each salinity value, where continuous measurements were performed using the calculated conservative (linear) values of temperature, TA and DIC between the two end-members in the main channel. We evaluated the impact of water heating on pCO_2 in the main channel and the secondary channel passing through the mangrove by normalizing the O-pCO_2 observed at a given salinity at the temperature corresponding to the linear interpolation of the temperatures in the freshwater and marine end-members. To that end, we calculated for each salinity point measurement, a temperature-normalized T-pCO_2 from the measured pCO_2, the conservative TA mixing line, and the lowest temperatures observed at each end-member, generally at night and early morning. In winter and neap tides (Aug. 2014), two distinct temperature marine end-members should be considered: one at the mouth of the main channel and another in the coastal lagoon at the mouth of the mangrove channel (Fig. 1). In contrast, a single set of freshwater and seawater temperature end-members could be used during summer and spring tides (Nov. 2015) when consistent cooler nighttime waters were observed in both marine end-members (see results section).

The evasion or invasion of CO_2 at the water-air interface was calculated according to:

$$FCO_2 = k\alpha\Delta pCO_2 \quad (1)$$

where FCO_2 is the water-air CO_2 flux (mol m^{-2} h^{-1}), k is the gas transfer velocity (m h^{-1}), α is the solubility coefficient (mol m^{-3} atm^{-1}), and ΔpCO_2 is the difference between water and air pCO_2 (in atm). Atmospheric pCO_2 was measured every morning and evening by pumping with the NDIR gas analyser, and daily average values were used for the flux calculation. To calculate k, we apply three equations as a function of the concomitant wind speed at 10 m (U10) recorded at a station located 4 km landward (Fig. 1). The equations of Wanninkhof, 1992 (referred to as W92) and Raymond and Cole (2001) (referred to as RC01) provide the gas transfer velocity as a function of U10, and the equation of Abril et al. (2009) (referred to as A09) provides the gas transfer velocity as a function of U10, estuarine surface area and water current velocity. In the A09 model, we used a surface area of 19 km^2 and an average water current of 0.4 m s^{-1} as representative for the São Francisco main channel (Cavalcante et al., 2017). For all calculations, pCO_2 and wind speed data were selected to calculate FCO_2 in winter and summer during the daytime and in summer at night.

To complete our study, we corrected the theoretical C-pCO_2 conservative mixing curves for the air-water CO_2 exchange, building Ex-pCO_2 curves. We applied an iterative calculation of every salinity unit from 0 to 34 of the loss or gain of DIC as CO_2 evasion or invasion during the mixing of water at salinity s with seawater to reach the value of salinity s + 1.

$$DICgain(s) = -FCO_2\,(s)RT.H^{-1} \quad (2)$$

where FCO_2(s) is the flux (mol m^{-2} h^{-1}), RT is the residence time (h) and H is the water depth (m). FCO_2(s) is calculated with Eq. (1) and the C-pCO_2 value at salinity s, deduced from the mixing of DIC(s) with DIC(34) and TA(s) with TA(34). Then, the new corrected DIC concentration at s + 1, DIC(s + 1), is obtained by adding the DICgain(s) to the DIC(s):

$$\text{Corrected DIC}(s+1) = DIC(s+1) + DICgain(s) \quad (3)$$

At that step, we recalculate a corrected C-pCO_2(s + 1) from the new mixing between corrected DIC(s + 1) and DIC(34) and TA(s + 1) and TA (34). The next iteration consisted of calculating the FCO_2(s + 1) from the corrected C-pCO_2(s + 1) and the DICgain(s + 2) using equation. The model was set up in the CO2sys spreadsheet (Pierrot et al., 2006), with each line representing a salinity increment of one unit, from zero to 34, with the possibility of choosing the gas transfer equation, U10, RT and H. Incrementation of the model allowed the building of thermodynamic Ex-pCO_2 mixing curves corrected from gas exchange according to various combinations of these parameters. We used an RT/H ratio of 0.17 day m^{-1}, which corresponds to a short RT value in the São Francisco estuary of 0.5 days as estimated from the discharge during the cruise, a mean H of 3 m and an estuarine surface of 19 km^2. To simulate conditions closer to those occurring in large river plumes, we also tested the influence of increasing RT/H to 0.33 and 0.5 day m^{-1}, and we applied three different wind speeds of 0.5, 3, and 7 m s^{-1} as representative of estuarine and shelf meteorological conditions. In addition, we assumed that the residence time was uniformly distributed along the salinity gradient, although there might be some exceptions, such as longer residence times (several tidal cycles) in the low salinity range.

3. Results

DIC and TA increased linearly with salinity in the main channel, from 553 ± 40 and 539 ± 27 μmol kg^{-1} in the river end-member to 1719 ± 127 and 1975 ± 146 μmol kg^{-1} at the mouth with salinity>30, respectively (Fig. 2). Some significant positive anomalies of both parameters were observed at high salinity stations in the mangrove channel (Fig. 2). During both cruises, O-pCO_2 was highly variable in the freshwater with some lateral heterogeneity between the different channels and was above the atmospheric pCO_2 at the centre of the main channel, with a value of ~700 ppmv (Fig. 3A&B). Downstream in the main channel, O-pCO_2 sharply decreased below 400 ppmv at salinity 3 and followed an asymmetric bell-shaped curve along the salinity gradient. In winter, the O-pCO_2 distribution in the main channel was almost perfectly predicted by thermodynamics during mixing, with the average difference between O-pCO_2 and C-pCO_2 in the 3–30 salinity range being 3 ± 13 ppmv (Table 1), that is, within the error of pCO_2 measurements and mixing model calculations. In summer, however, O-pCO_2 in the main channel was on average 43 ± 35 ppmv above the theoretical mixing curve of C-pCO_2 along the 3–30 salinity range at night and daytime. The measured O-pCO_2 included undersaturated values and invasion of atmospheric CO_2 at salinities above 3 during both cruises (Fig. 3A&B). Most marine waters with salinities >30 were undersaturated in Aug. 2014 (O-pCO_2: 332 ppmv) and almost at equilibrium (O-pCO_2: 403 ± 18 ppmv) in Nov. 2015 (Fig. 3E&F). In the mangrove channel, O-pCO_2 was higher and more variable than in the main channel: between 298 and 975 ppmv (mean 512 ppmv) in winter and between 307 and 2007 ppmv (mean 976 ppmv) in summer (Fig. 3A&B). Several O-pCO_2 peaks occurred in the mangrove channel, and the adjacent coastal lagoon at intermediate and high salinities, and variations also occurred according to the tidal phase, with higher values in Nov. 2015 corresponding to low tide during the spring tide period. A

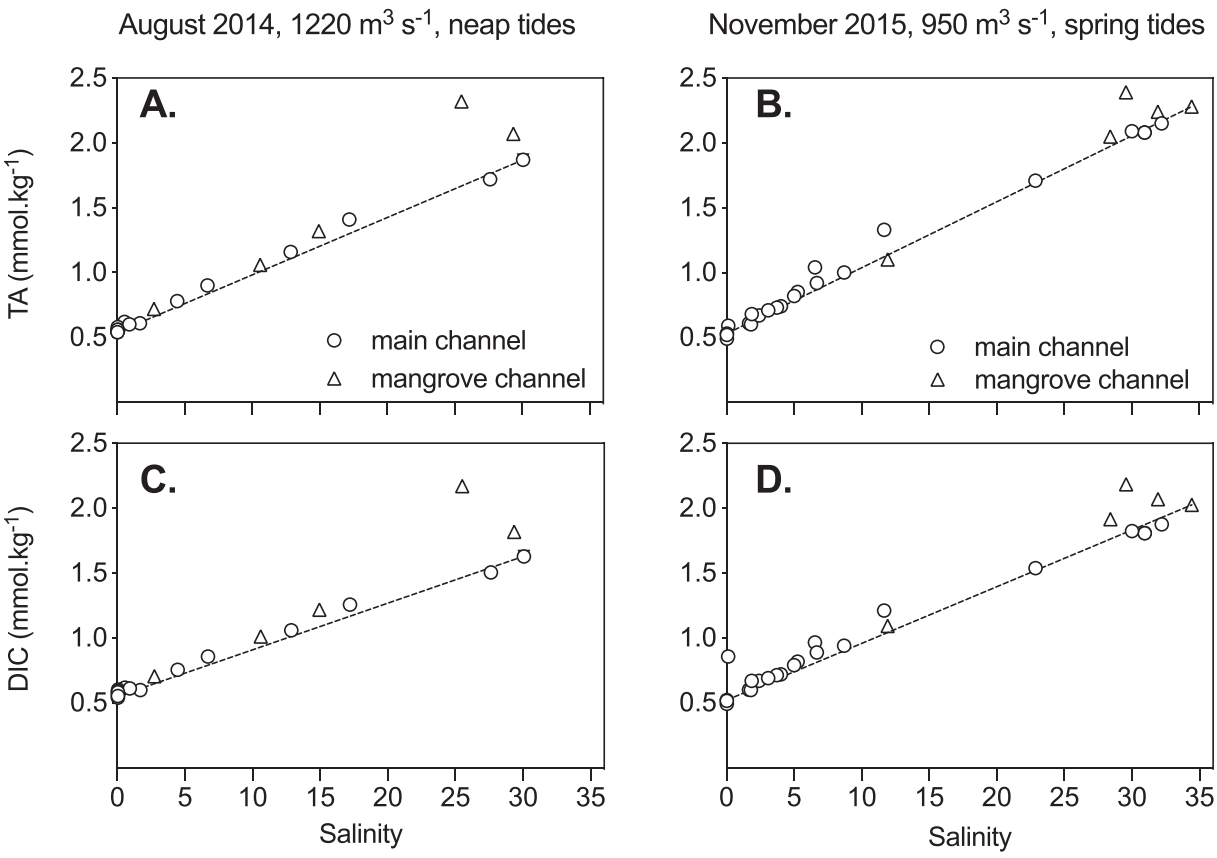

Fig. 2. Distribution of Total Alkalinity (TA) (A. and B.) and Dissolved Inorganic Carbon (DIC) (C. and D.) concentrations as a function of salinity in the São Francisco estuary main channel (circles) and mangrove secondary channel (triangles) in August 2014 (A. and C.) and November 2015 (B. and D.).

maximum of 2000 ppmv was recorded in the coastal lagoon at the outlet of the mangrove channel during the afternoon at low tide (Fig. 3B). During the two cruises, DO remained between 99% and 101% saturation throughout most of the salinity gradient in the main channel (Fig. S2). In both seasons, significant DO undersaturation occurred in the river at low salinities and in the mangrove channel, with lower minimum values in Nov. 2015 than in Aug. 2014. In Nov. 2015, slight DO oversaturation (max 103%) was observed in the main channel at salinities of approximately 3 and above 31 (Fig. S2).

Water temperatures were lower in Aug. 2014 than in Nov. 2015 (Fig. 3C&D). During winter and neap tides (Aug. 2014), the temperature remained constant in the main channel and approximately 1 °C above the conservative mixing line in the mangrove channel, showing that water heating occurred (Fig. 3C). In Aug. 2014, O-pCO_2 was 5–20 ppmv higher than T-pCO_2 in the mangrove channel but less than 2 ppmv in the main channel (Fig. 3E). In Nov. 2015, when measurements were also performed at night, surface heating was evident from nighttime to daytime, as well as within the mixing zone in comparison with the two end-members. The entire salinity gradient in both channels was more than 1 °C cooler at night and early morning (before 9 h) than at daytime and dusk (Fig. 3D), which resulted in O-pCO_2 being higher than T-pCO_2 by 10–15 ppmv (Fig. 3F). A peak temperature of 29.8 °C occurred in Nov. 2015 during the afternoon in the shallow lagoon at the outlet of the mangrove channel at low tide, which corresponded to an O-pCO_2 120 ppmv higher than T-pCO_2 when the O-pCO_2 reached 2000 ppmv (Fig. 3F).

During the 25 h cycle at the anchored station in the main channel on the 11th and 12th of Nov. 2015, salinity varied between 1.2 and 32.2, and water pCO_2 varied between 238 ppmv at intermediate salinities and 476 ppmv at low salinity. The record at one-minute frequency revealed remarkable parallelism between O-pCO_2 and C-pCO_2 calculated from mixing the two end-members and the salinity value. However, O-pCO_2 was on average + 43 ± 35 ppmv above the conservative mixing curve of C-pCO_2 (Fig. 4). Maximum deviations of O-pCO_2 from C-pCO_2 occurred during the ebb tides, both at sunset and night (hours 1.5 to 4.2: 52 ± 19 ppmv) and at sunrise and early morning (hours 13.5 to 17.5: 92 ± 30 ppmv). In addition, at low tide when salinities were below 3, O-pCO_2 values were close to the C-pCO_2 during the daytime (hours 19–21.5) but were ~ 60 ppmv higher than C-pCO_2 at night (hours 7–10), indicating diurnal variations in this low salinity range (Fig. 3). Finally, throughout the 25 h cycle, some heating effect on pCO_2 was detected during the afternoon at high tide and high salinity (hours 1 and 25) and at low tide and low salinity (hour 20), when O-pCO_2 was at a maximum +25 ppmv higher than T-pCO_2 (Fig. 4B).

Wind speed was low during the cruises, always below 3.5 m s^{-1}, on average between 1.1 m s^{-1} in Nov. 2015 and 2.2 m s^{-1} in April during the daytime, and 0.5 m s^{-1} at nighttime (Table 1). In the main channel, FCO_2 fluxes varied between 0.01 and 0.79 mmol m^{-2} h^{-1} (positive fluxes for CO_2 evasion) in the 0–3 salinity range and between −0.04 and − 1.68 mmol m^{-2} h^{-2} in the 3–30 salinity range. In the mangrove channel, the calculated FCO_2 varied between 1.23 and 10.72 mmol m^{-2} h^{-1}. For the observed wind speed range, the calculated FCO_2 strongly depended on the choice of the k_{600} parameterization, and the W92 equation gave lower fluxes than the RC01 and A09 equations (Table 1).

Ex-pCO_2, the theoretical thermodynamic pCO_2 mixing curves corrected for gas exchange, were below the standard conservative curve between salinities 0 and 3–5, where CO_2 evasion occurs, and above the curve between salinities 3–5 and 34, where the invasion of atmospheric CO_2 occurs (Fig. 5). Computed deviation from conservative mixing, i.e., Ex-pCO_2 minus C-pCO_2, strongly depended on the selected parameters, the gas transfer parametrization, U10 and the residence time/depth ratio. These deviations varied from −0.3 to −167 ppmv (average − 29

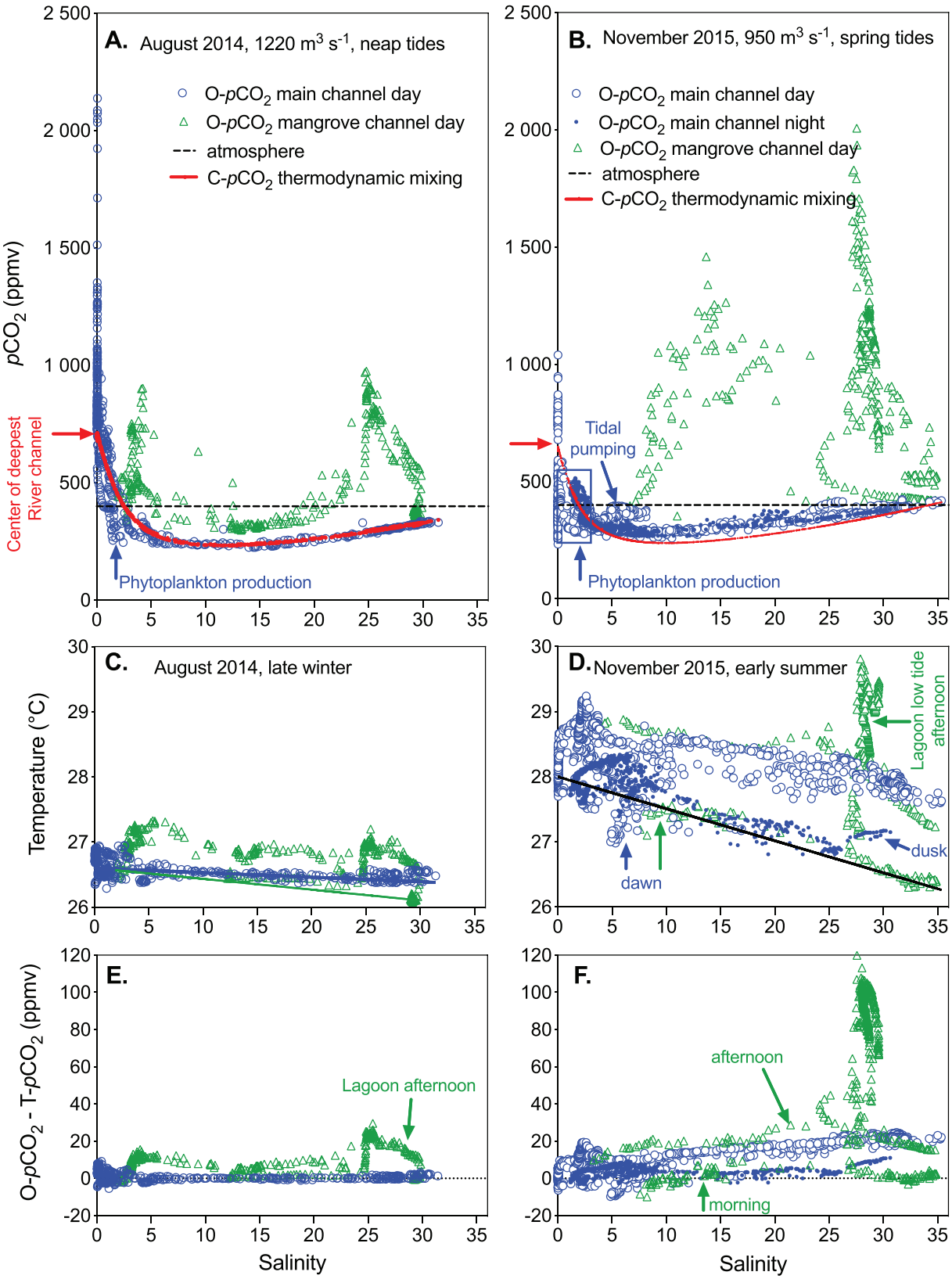

Fig. 3. Distribution of O-pCO_2 (A. and B.), temperature (C. and D.), and the difference between O-pCO_2 and T-pCO_2 (E. and F.) versus salinity in the São Francisco Estuary main channel (blue circles) and mangrove secondary channel (green triangles). The regression lines in panel C indicate the conservative mixing for temperature used for pCO_2 temperature normalization in the main channel (blue) and in the secondary mangrove channel (green) with a distinct marine end-member in the lagoon. The black regression line in panel D indicates the conservative mixing for temperature in the main channel and in the secondary mangrove channel with the same values in both marine end-members (see "results"). (For interpretation of the references to colour in this figure legend, the reader is referred to the web version of this article.)

Table 1
Synthesis of measured and calculated parameters during the two cruises. O-pCO_2 is the observed pCO_2 as measured in situ, C-pCO_2 is the conservative pCO_2 modelled from mixing of river water with seawater, T-pCO_2 is the pCO_2 normalized to temperature resulting from the mixing of the two end-members and Ex-pCO_2 is the pCO_2 resulting from conservative after being corrected for gas exchange.

	Aug. 2014			Nov. 2015				
	Main channel		Mangrove	Main channel				Mangrove
	S < 3	S > 3	S > 3	S < 3		S > 3		S > 3
	Day	Day	Day	Day	Night[b]	Day	Night	Day
Number of measurements	321	190	324	518	260	701	441	528
Temperature (°C)	26.6 ± 0.2	26.5 ± 0.1	26.7 ± 0.4	28.3 ± 0.4	27.9 ± 0.2	28.1 ± 0.4	27.7 ± 0.5	28.3 ± 0.9
	26.1–27.0	26.4–26.7	26.1–27.3	27.5–29.2	27.6–28.2	27.0–28.9	26.8–28.4	26.3–29.8
O-pCO_2 (ppmv)	752 ± 308	279 ± 34	512 ± 191	426 ± 141	421 ± 60	344 ± 39	311 ± 30	976 ± 314
	245–2137	224–355	298–975	233–1040	304–514	259–423	267–383	307–2007
C-pCO_2 (ppmv)	634 ± 92	282 ± 33	296 ± 36	542 ± 123	392 ± 34[a]	295 ± 46	275 ± 31	334 ± 41
	371–710	233–343	232–368	318–646	298–476	238–411	238–363	238–406
T-pCO_2 (ppmv)	753 ± 311	279 ± 34	503 ± 185	421 ± 144	420 ± 61	332 ± 37	307 ± 29	917 ± 292
	245–2166	224–357	293–949	228–1043	299–512	252–405	264–373	297–1956
Ex-pCO_2 (ppmv)	622 ± 95	284 ± 34	–	530 ± 125	386 ± 36[a]	299 ± 47	280 ± 32	–
	357–692	236–344		307–635	294–472	238–411	241–369	
O-pCO_2 – C-pCO_2 (ppmv)	117 ± 256	−3 ± 13	216 ± 180	−104 ± 90	29 ± 21	49 ± 39	36 ± 22	643 ± 320
	−243-1444	−65-69	40–680	−413-407	−64-101	−31-141	−41-111	−11 − 1671
O-pCO_2 – T-pCO_2 (ppmv)	-1 ± 7	0 ± 1	9 ± 8	5 ± 7	2 ± 2	12 ± 8	5 ± 3	59 ± 40
	−29-9	−2-3	−1-30	−6-19	−3-6	−10-25	−3-11	−10 − 124
O-pCO_2 – Ex-pCO_2 (ppmv)[a]	−12 ± 9	2 ± 2	–	-12 ± 9	−6 ± 3	4 ± 3	4 ± 3	–
U_{10} (m s^{-1})	1.1 ± 0.7	1.1 ± 0.7	0.6 ± 0.4	2.2 ± 1.0	0.4 ± 0.2	2.2 ± 1.0	0.4 ± 0.2	1.1 ± 0.5[c]
	0.1–2.8	0.1–2.8	0.5–1.4	0.9–3.2	0.1–1.1	0.9–3.2	0.1–1.1	0.5–1.6[c]
k_{600} (cm h^{-1}) W92	0.6	0.6	0.2	1.6	0.1	1.6	0.1	0.5
k_{600} (cm h^{-1}) RC01	3.4	3.4	2.9	4.1	2.2	4.1	2.2	2.8
k_{600} (cm h^{-1}) A09	5.6	5.6	4.1	7.3	2.8	7.3	2.8	4.6
FCO_2 W92 (mmol m^{-2} h^{-1})	0.74 ± 0.30	−0.25 ± 0.03	0.09 ± 0.03	0.18 ± 0.06	0.01 ± 0.00	−0.38 ± 0.04	−0.04 ± 0.00	1.23 ± 0.40
FCO_2 RC01 (mmol m^{-2} h^{-1})	3.93 ± 1.61	−1.35 ± 0.17	1.05 ± 0.39	0.44 ± 0.15	0.19 ± 0.03	−0.94 ± 0.11	−0.78 ± 0.07	6.55 ± 2.11
FCO_2 A09 (mmol m^{-2} h^{-1})	6.43 ± 2.64	−2.21 ± 0.27	1.48 ± 0.55	0.79 ± 0.26	0.24 ± 0.03	−1.68 ± 0.19	−1.01 ± 0.10	10.72 ± 3.45

[a] Calculated using the mixing/gas exchange model described in Fig. 5, for the measured U10, a value of RT of 0.5 days and H of 3 m.
[b] During night, measured and modelled conservative pCO_2 values are lower than expected when compared to the daytime, because night-time measurements did not include samples with salinities lower than 1.2 and highest pCO_2.
[c] In order to account for the protection of mangrove trees to creek waters, we divided by 2 the wind speed values to calculate CO_2 fluxes from the mangrove secondary channel, as a first approximation. Standard deviation of the differences between two numbers were calculated as the square root of the sum of the squares of the two errors.

ppmv) in the 0–3 salinity range and from −8 to +76 ppmv (average + 16 ppmv) in the 3–30 salinity range. Applying a residence time in the São Francisco estuary of 0.5 days during the cruises, an average water depth of 3 m and U10 values of 0.5 and 3 m s^{-1} as representative for the conditions during the cruise gives Ex-pCO_2 - C-pCO_2 values of −12 ± 9 ppmv in the 0–3 salinity range and 4 ± 3 ppmv in the 3–30 salinity range (Table 1).

4. Discussion

4.1. Predominance of thermodynamics

In the main channel, the pCO_2 measurements (O-pCO_2) and the thermodynamic estuarine conservative mixing model (C-pCO_2) follow the same asymmetric bell-shaped curve, with a steep decrease from salinity zero to 3 and undersaturation of surface waters along the 3–30 salinity gradient (Fig. 3). To date, such well-defined pCO_2 curves, with high-resolution measured values that are very consistent with the theoretical conservative mixing curve, have been reported in the Amazon plume only for salinities higher than 17 and in the tropical Paraiba do Sul along the entire salinity gradient, with continuous pCO_2 measurements (Cotovicz Jr. et al., 2020). In the mesotrophic Paraiba do Sul River Estuary, autotrophic and heterotrophic activities strongly influenced the pCO_2 distribution along the salinity gradient at low river discharge but not at high discharge and shorter residence time, when the pCO_2 versus salinity plot followed the theoretical curve (Cotovicz Jr. et al., 2020). Because of the oligotrophic character of the São Francisco estuary (Medeiros et al., 2011, 2018) and the short residence time of water in the mixing zone (half a day), thermodynamics predominate over biological processes in controlling estuarine pCO_2 distribution along the estuarine gradient. Some theoretical works have described how thermodynamics during estuarine mixing can generate positive or negative air-water CO_2 fluxes depending on the DIC and TA concentrations in the river end-member, and the concentrations in the marine end-member are considered constant in comparison (Whitfield and Turner, 1986; Cai et al., 2013; Delaigue et al., 2020). In the case of São Francisco with a low TA river end-member (approximately 500 μmol kg^{-1}) and warm waters (above 25 °C), thermodynamics during mixing turn the estuary into a sink of atmospheric CO_2 (Whitfield and Turner, 1986); this is also the same for the Amazon (TA of 450 μmol kg^{-1}) and Congo (300 μmol kg^{-1}) but not the Mississippi (>2000 μmol kg^{-1}), where carbonate thermodynamics generate a CO_2 source and where the observed CO_2 invasion is biological, as revealed by nitrate uptake (Cai et al., 2013). Although the conditions found in the largest world rivers potentially generate a CO_2 sink in the coastal zone, very few in situ pCO_2 data cover a complete estuarine salinity gradient consistent with the pCO_2 theoretical mixing curve (Cai et al., 2013; Lefèvre et al., 2017; Cotovicz Jr. et al., 2020). In winter in the São Francisco estuary, the average difference between O-pCO_2 and C-pCO_2 was only 3 ± 13 ppmv along the 3–30 salinity range in the main channel, and thermodynamics was apparently the unique driver of the carbonate system, creating a permanent CO_2 influx in this salinity range. In summer, the average difference between O-pCO_2 and C-pCO_2 at salinities >3 was +49 ± 39 ppmv during the daytime and + 36 ± 22 at night (Table 1), but O-pCO_2 always remained below the atmospheric value of 400 ppmv at salinities above 3, and the thermodynamic uptake of atmospheric CO_2 was predominant.

Our continuous measurements in São Francisco also allow an interpretation of these O-pCO_2 deviations from C-pCO_2 as the result of other internal CO_2 sources and sinks. First, estuarine NEP and lateral transport

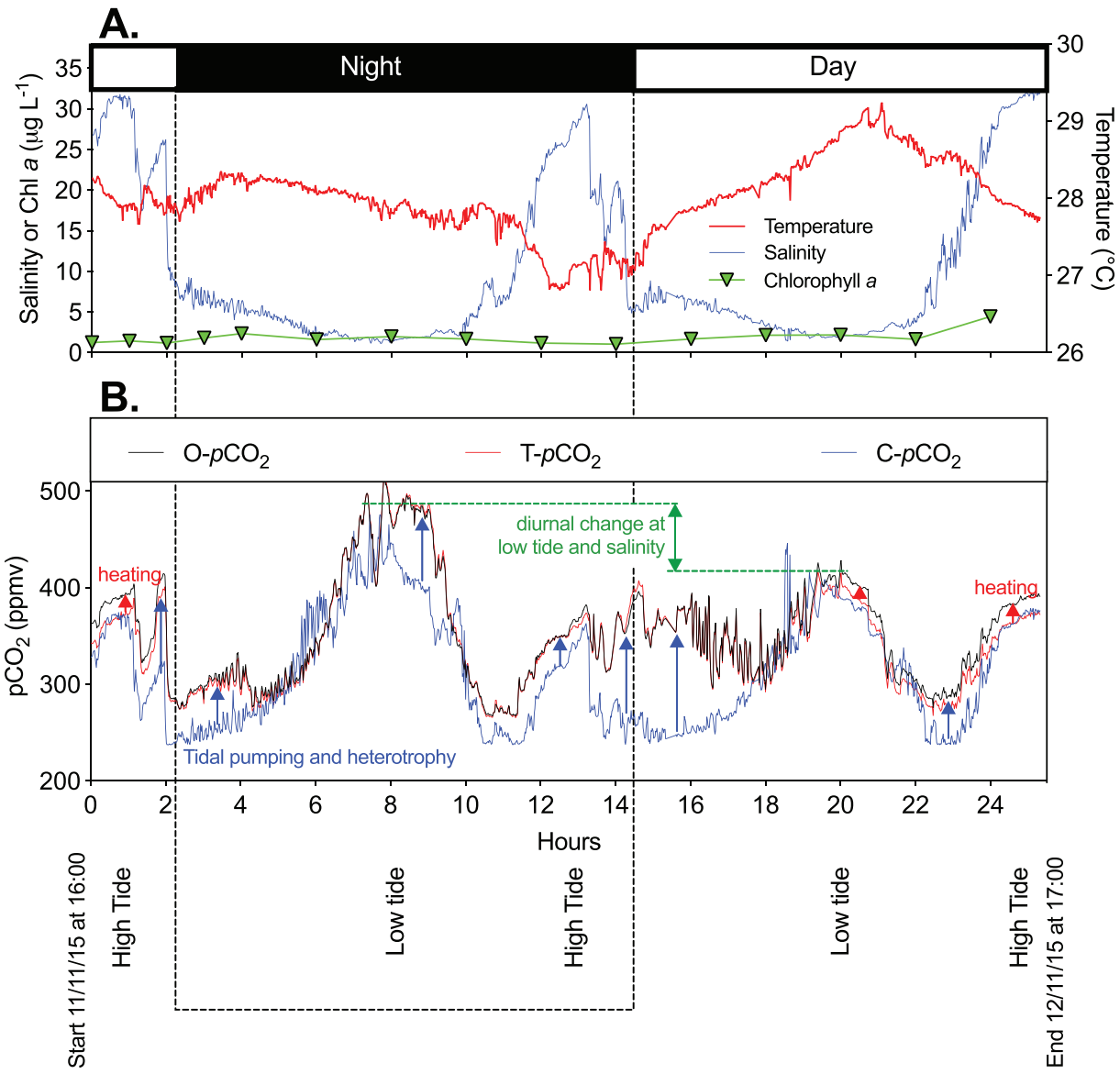

Fig. 4. Time course of physico-chemical parameters in surface water of the main channel of the São Francisco River Estuary during the 25 h cycle in Nov. 2015 (summer and spring tides). (A.) Temperature and Salinity and (B.) measured O-pCO_2 (black line), temperature-normalized T-pCO_2 (red line), and the C-pCO_2 induced by conservative mixing of seawater with freshwater calculated from the salinity record (blue line). Upward blue arrows indicate the occurrence of tidal pumping, net heterotrophy and gas exchange (invasion of atmospheric CO_2). Upward red arrows indicate the impact of heating on pCO_2. Green double arrows indicate the significant diurnal change in low salinity waters. (For interpretation of the references to colour in this figure legend, the reader is referred to the web version of this article.)

from the river and intertidal areas can be sources of CO_2 (Borges and Abril, 2011; Bauer et al., 2013). Second, C-pCO_2 simulations were based on the conservative mixing of temperature during the daytime at the two end-members. However, heating and cooling of water is a common feature in this semiarid region and can potentially change pCO_2 at daily and tidal time scales, particularly in shallow regions of the estuary such as the lagoon. Third, while the air-water exchange of CO_2 is much slower than acid-base equilibration of DIC species, evasion and invasion of CO_2 occur during estuarine mixing, potentially altering the thermodynamic pCO_2 curve. All these processes can generate pCO_2 changes of a few tens of ppmv that can add up to the values of pCO_2 deviations from the mixing curves in summer (Cotovicz Jr. et al., 2020). However, when interpreting these deviations, we must also keep in mind that the shape of the modelled C-pCO_2 curve depends on the choice of the freshwater end-member, which was difficult to define because of lateral heterogeneity. For example, we calculated that using a freshwater end-member with 5 µmol kg^{-1} higher TA (or DIC) (a change within the range of analytical precision for these parameters) generates mixing pCO_2 values 10 ppmv lower (or 9 ppmv higher) at salinity 10. In the case of our study, we choose to use the TA and pCO_2 values at the central and deepest station upstream of all the small islands (Fig. 1), where most freshwater flows and with little tidal influence, and not an average of all measurements at the lowest salinity (<0.1) region. Owing to the significant heterogeneity in the different canals, we cannot exclude lateral input of freshwater from small tributaries in this region that alter the DIC concentrations in the end-member and the modelled mixing pCO_2 curve.

4.2. *Biological CO_2 sources and sinks*

The diurnal O-pCO_2 change at low salinity (Fig. 4) reveals some photosynthetic activity in this region, despite the Chl *a* concentration of approximately 3 µg L^{-1} (Fig. 4). During our measurements (Fig. 4), the respiration of this plankton apparently generated a deviation of +60 ppmv above the conservative mixing at night and early morning (hours

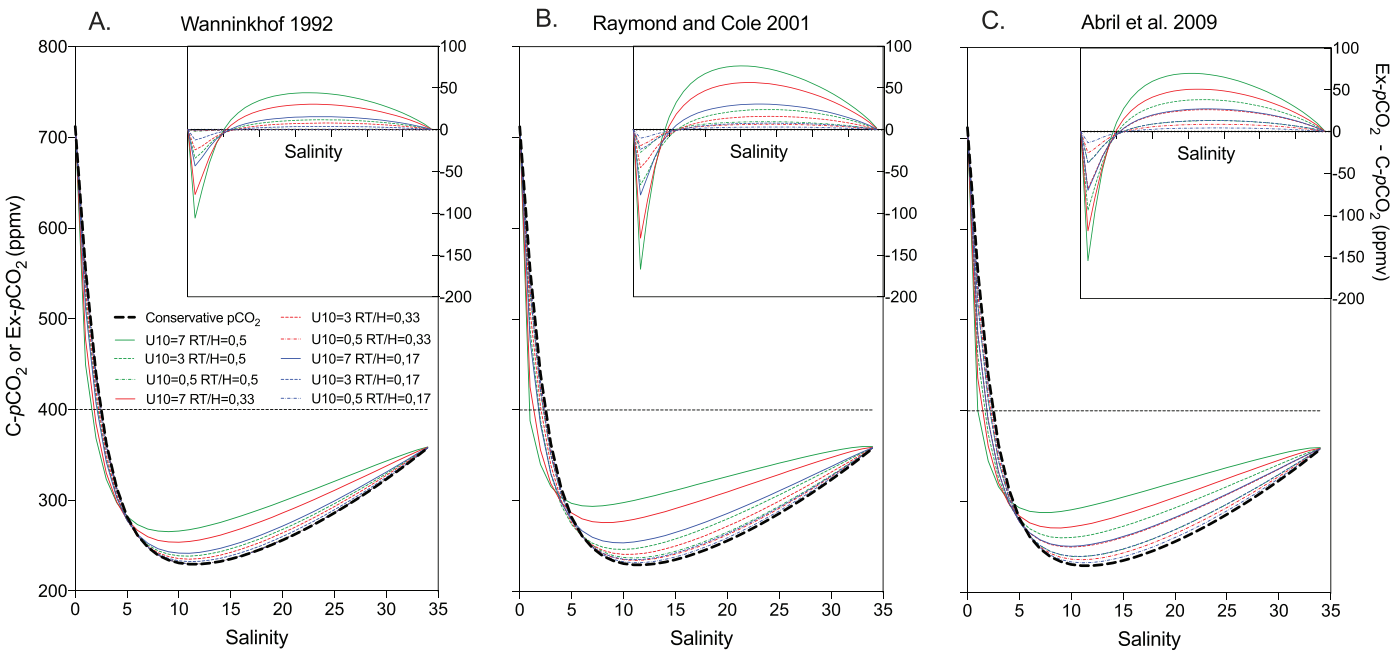

Fig. 5. Impact of air-water CO_2 exchange on thermodynamic conservative pCO_2 mixing curves. Calculations were made using Temperature, Salinity, DIC and TA observed in the freshwater and marine end-members in Nov. 2015 and the gas exchange was computed every salinity unit increment (see Section 2.2). RT/H is the ratio between residence time and water depth, and the selected value of 0,17 is representative for estuarine systems such as the São Francisco, whereas the value may apply to larger tropical rivers such as the amazon or congo.

7–9) compared to the afternoon when phytoplankton absorbed CO_2 (hours 21–23). Concomitant changes in DO could be detected, although the DO values remained very close to 100% at night and daytime in the whole salinity range. We calculated that for the conditions of Nov. 2015, the diurnal change of 60 ppmv of O-pCO_2 at salinity 3 corresponds to a change in DIC of 5 μmol kg^{-1}. If we assume a photosynthetic/respiratory quotient of 1, the equivalent diurnal change in DO in these oligotrophic waters would be approximately 2%sat. In fact, in Nov. 2015, the DO concentration at salinity 3 was 100% at night, and 103% at daytime (Fig. S2), but these differences remained close to the error in DO measurements. Consequently, pCO_2 monitoring was much more powerful than O_2 monitoring to detect photosynthetic activity in the oligotrophic São Francisco estuary. It is well known that freshwater phytoplankton can still be active in estuaries at low salinities but generally not at higher salinities in the mixing zone, where they die due to saline stress (Lancelot and Muylaert, 2012). This is probably the case in the São Francisco estuary, where despite the general low biomass, freshwater phytoplankton potentially fuel heterotrophy downstream in the main channel. However, the residence time of half a day is probably too short to allow the establishment of an active heterotrophic community (Crump et al., 2004). Benthic heterotrophy is probably limited in the sandy sediments of the São Francisco estuary, where strong hydrodynamics limit the deposition of fine organic biodegradable material (Medeiros et al., 2007). Along the salinity gradient, the deviation of O-pCO_2 from C-pCO_2 was spatially and temporally linked to tidal advection from mangroves and other brackish marshes. Many authors have reported high CO_2 degassing fluxes from mangrove surrounding waters (Borges et al., 2003; Maher et al., 2013; Santos et al., 2018; Cotovicz Jr. et al., 2020). High water pCO_2 comes from the tidal pumping of mangrove-saturated soil CO_2 (Maher et al., 2013; Santos et al., 2018) and from the respiration of mangrove-derived organic matter in creek waters and sediments (Bouillon et al., 2003; Borges and Abril, 2011). In mangrove soils, a large part of the metabolism is sulfate reduction, which stoichiometrically produces the same amount of TA as CO_2 (Borges et al., 2003). This explains the positive TA (and associated DIC) anomalies observed at high salinities in the mangrove channel of the São Francisco Estuary (Fig. 2). Although water O-pCO_2 was similar during both campaigns in the main channel, pCO_2 values were much higher in the secondary channel, particularly in Nov. 2015 compared to Aug. 2014. This can be attributed to the spring tide conditions during sampling in 2015, enhancing tidal pumping (Maher et al., 2013; Santos et al., 2018). During the 25 h cycle in the main channel at spring tide in 2015 (Fig. 4), the highest (>100 ppmv) and longest positive deviations of O-pCO_2 from C-pCO_2 occurred during the ebb tides, particularly at late night and early morning (hours 14–17), which reveals an export from the mangrove waters to the main channel that affects the 5–8 salinity range (Fig. 3B). The monitoring point over 25 h was located less than two km from the confluence between the main channel and the mangrove channel and close to brackish tidal marshes (Fig. 1), which could contribute, together with mangroves, to the pCO_2 peaks at high and ebb tides. In addition, the short residence time of waters in the estuary suggests that heterotrophs would spend little time in the main channel and would be exposed to strong salinity stress to generate significant respiratory CO_2, which apparently comes in majority from tidal pumping.

4.3. *Impact of heating*

Semiarid coastal ecosystems are environments where heating and evaporation can have a strong influence on water chemistry, and very few studies document the behaviour of carbonate system (Leopold et al., 2016; Yao and Hu, 2017; Yao et al., 2020). Heating of water first increases the pCO_2 and favour outgassing (Takahashi et al., 2002). If evaporation is intense and leads to hypersaline conditions, TA consumption and CO_2 release due to carbonate precipitation can occur (Murgulet et al., 2018; Yao et al., 2020). In the São Francisco estuary, higher temperatures relative to the mixing of the two end-members were most pronounced during summer and in the mangrove secondary channel (Fig. 3C&D). In summer, despite the short residence time of waters, the temperature increased in both channels by more than 1 °C during the daytime compared to the nighttime (Fig. 3D), which corresponds to a theoretical pCO_2 increase (difference between O-pCO_2 and T-pCO_2) of ~15 ppmv (Fig. 3F). In the main channel, the 25 h cycle (Fig. 4) reveals that heating during the daytime has a significant impact

on pCO_2 at both low tide (hour 21) and high tide (hours 1 and 25). In Nov. 2015, at salinities >3, the average observed pCO_2 in the main channel in summer was 33 ppmv higher during the daytime than during the nighttime, and the thermal effect contributed to 25% of the deviation in pCO_2 above the conservative curve during the daytime and to 10% of the deviation in pCO_2 above the conservative curve during the nighttime when estuarine waters remained warmer than predicted due to the mixing of the end-members (Table 1). At salinities <3, the thermal effect was partially offset by biological productivity, and the O-pCO_2 was similar at night and daytime. However, the daytime data included salinities below 1.4 with higher O-pCO_2, whereas nighttime data did not (Table 1). In the secondary channel, the maximal thermal effect occurred at salinity ~28 in the coastal lagoon in the afternoon at low tide, with an increase in temperature of ~3 °C concomitant with a maximum pCO_2 of ~2000 ppmv (Fig. 3C, F). The thermal effect at this site (Fig. 3F) contributed to 15% of the deviation of pCO_2 above the conservative curve at maximum (Fig. 3B), and this pCO_2 peak is attributed to the maximum pumping of mangrove-derived CO_2 at low tide. Although the water depth was less than half a metre and the temperature reached 29.8 °C, we found no evidence of carbonate precipitation during this event, similar to those reported in other semiarid coastal lagoons (Yao et al., 2020). Indeed, the salinity was only 28 during the pCO_2 peak and increased only when the tide started to enter the system through the small canals (Fig. 1); no significant TA consumption could confirm carbonate precipitation. TA was above the mixing line in this region due to tidal pumping of DIC from predominant sulphate reduction and other anaerobic processes in the mangrove soils (Borges et al., 2003; Santos et al., 2018).

4.4. Impact of gas exchange

The fact that thermodynamic mixing in the main channel generates undersaturated pCO_2 conditions with respect to the atmosphere implies that uptake of atmospheric CO_2 occurs at salinities >3. Consequently, the hypothesis of conservative DIC mixing on which the thermodynamic pCO_2 curve relies becomes invalid, whereas that of conservative TA remains valid. If we consider the average and standard deviation air-water CO_2 fluxes calculated with the conservative pCO_2 mixing curve and the three gas exchange equations (Table 1), then thermodynamics during mixing in the main channel emit $+2.5 \pm 1.7$ mmol m^{-2} h^{-1} of CO_2 at salinities lower than 3 and absorb -1.3 ± 0.6 mmol m^{-2} h^{-1} of CO_2 between salinities 3 and 34. Precise integration of these fluxes would require an estimate of the relative surface area of different salinity ranges according to the shape of the pCO_2 bell curve. In particular, it is necessary to separate the 0–3 salinity range that behaves as a source (as does the river) from the estuarine waters with salinities above 3 that behave as a sink (Table 1). During our study, we sampled the marine end-member in the shallow waters of the mouth of the estuary at high tide (Fig. S1). However, at low tide and on average over the tidal cycle, salinity at the mouth is generally lower, and a significant part of the salinity gradient occurs in a plume offshore. Based on numerical modelling, Cavalcante et al. (2020) showed that the tide-integrated salinity at the mouth of the São Francisco Estuary could be as low as 22 during concomitant neap tides and high river flow. In addition, surface waters with salinities lower than 34 extend 5–20 km offshore, with a surface area up to 50 km^2, an area much larger than the 19 km^2 of the inner estuary (Cavalcante et al., 2020). Considering the low river discharge during the study period, an area of 6 km^2 for the 0–3 salinity range, which corresponds to one-third of the inner estuary, emits 4.3 tC per day. An area of 30 km^2 (13 km^2 in the inner estuary and 17 km^2 in the plume offshore) for the 3–34 salinity range absorbs −11.2 tC per day. With these hypotheses on the surface areas, the São Francisco Estuary absorbs 7 tC per day of CO_2. In comparison, the input of DIC by the river was 95 and 70 tC per day in Aug. 2014 and Nov. 2015, respectively. Consequently, the invasion of CO_2 from the atmosphere due to thermodynamics during mixing increases the DIC export to the sea by 7–10%. This modest increase in the DIC discharge of the São Francisco Estuary to the ocean might also be partly explained by the morphology and hydrological features induced by very shallow depths at the mouth and a very steep longitudinal salinity gradient between 10 and 25 inside the lagoon (Fig. 4).

By calculating the quantity of CO_2 absorbed from the atmosphere during the residence time of waters in the estuary for each salinity increment, our mixing Ex-pCO_2 model provides a precise evaluation of the impact of gas exchange on the C-pCO_2 curves (Fig. 5). Evasion occurs first at low salinity, and the correction is negative during a limited amount of time; invasion occurs at salinities above 3–5 with a positive correction and presumably during a longer amount of time. In the case of the São Francisco Estuary, with a water depth of 3 m, a residence time of half a day and relatively low wind speed values (Table 1), the model results in a difference between C-pCO_2 and Ex-pCO_2 of only 4 ppmv in the 3–30 salinity range in Nov. 2015, corresponding to ~10% of the O-pCO_2 deviation above the C-pCO_2 mixing curve. However, strong stratification of the water column at intermediate salinities may alter this conclusion in two opposite ways: on the one hand, if we consider a mixed surface layer of only 1 m height as representative in situ conditions (Cavalcante et al., 2017), CO_2 invasion would generate a larger difference between Ex-pCO_2 and C-pCO_2, on average ~ 12 ppmv, which corresponds to ~25% of the O-pCO_2 deviation above the C-pCO_2 mixing curve at salinity >3 in Nov. 2015; on the other hand, stratification of the water column implies that part of the mixing of estuarine water occurs below the water surface, that is, without contact with the atmosphere and without gas exchange. Wind speed, fetch length, and water current all contribute to surface turbulence in estuaries, where gas exchange is generally faster than in the ocean (Borges et al., 2004; Orton et al., 2010). Most of the proposed k_{600} parameterizations in estuaries are based on data in relatively well-mixed estuaries (Borges et al., 2004; Abril et al., 2009; Orton et al., 2010). To the best of our knowledge, no gas exchange study has been performed in highly stratified systems, where buoyancy fluxes dissipate kinetic energy as turbulence (Etemad-Shahidi and Imberger, 2002) potentially enhances gas exchange. In contrast, stratification limits the vertical diffusion of atmospheric CO_2 to the whole water column. In large tropical estuaries and plumes such as the Amazon and the Congo, most of the salinity gradient occurs offshore where wind speed is higher. Gas exchange in these plumes can significantly alter the C-pCO_2 mixing curves, and the impact of stronger wind and longer residence time in the mixing zone might be partially offset by a deeper mixed layer in the range of 5–30 m (Grodsky et al., 2014; Phillipson and Toumi, 2020).

4.5. Relative contributions of pCO_2 deviations from conservative mixing

In August 2014, in the main channel of the São Francisco estuary, heating and tidal pumping were almost negligible. We found a little deviation of O-pCO_2 from C-pCO_2, except in the salinity range 0–3, where the O-pCO_2 was on average 45 ppmv lower than the modelled conservative pCO_2 (Fig. 3A), suggesting the occurrence of autotrophic activity by phytoplankton and/or CO_2 evasion in the area, consistent with observations at low tides in Nov. 2015 during the 25 h cycle (Fig. 4). In contrast, the deviation from conservative mixing was more pronounced in Nov. 2015 during summer and spring tides. We could calculate the distribution of the three major active processes that make pCO_2 deviate from the conservative curve along the salinity gradient, that is, (i) surface water heating or cooling based on temperature field data (T-pCO_2), (ii) evasion or invasion of CO_2 based on modelling (Ex-pCO_2), and (iii) autotrophy or the sum of heterotrophy and tidal pumping from mangrove creeks as the residual part of the deviation between modelled and observed data, calculated as O-pCO_2 – T-pCO_2 – Ex-pCO_2 (Cotovicz Jr. et al., 2020). We binned our November 2015 data and calculated the means and standard deviations of O-pCO_2 and T-pCO_2 for each salinity increment. In August 2014, the deviation of pCO_2 from conservative mixing was too low (Table 1). The differences between O-

pCO_2, C-pCO_2, T-pCO_2, and Ex-pCO_2, were within the uncertainties of measurements and calculations, meaning that thermodynamics alone drives almost all the O-pCO_2 distribution. The 2015 binned O-pCO_2 and T-pCO_2 could be compared with the modelled C-pCO_2 and Ex-pCO_2 (Fig. 6). We also separated the day and night periods for the regions with salinities above and below 3. We calculated the CO_2 fluxes corresponding to these three processes (heating, gas exchange and the residual as biological activity) using wind speed data and three gas transfer parameterizations (Table 2). The calculations indicate that in Nov. 2015, heating was consistently stronger during the daytime than at night and contributed to a peak at 20 ppmv at salinity 28 (Fig. 6) and a maximum average deviation from conservativity of +12 ppmv during the daytime and salinity above 3, corresponding to a heating CO_2 flux of 0.2 mmol m^{-2} h^{-1} (Table 2). The gas exchange had a slightly lower impact on pCO_2 values than heating, with rapid evasion of river-borne CO_2 occurring at low salinity and CO_2 invasion at salinities between 3 and 34. According to our quantitative analysis, concomitant CO_2 evasion and net autotrophy occur in the 0–3 salinity range, whereas concomitant CO_2 invasion and net heterotrophy associated with tidal pumping from mangroves occur at salinities above 3 (Fig. 6). This trend in the São Francisco Estuary is similar to that recently reported in the mesotrophic Paraiba do Sul Estuary during high river discharge (Cotovicz Jr. et al., 2020). These two river-dominated tropical estuaries have low TA concentrations in the river end-member. At low salinities, inputs of river-borne CO_2 combined with low buffering capacity favour outgassing, whereas little salinity stress allows some production of freshwater phytoplankton (Cloern, 1996; Lancelot and Muylaert, 2012; Cotovicz Jr. et al., 2020). At salinities below 3, the O-pCO_2 values were 109 ppmv below the modelled C-pCO_2 values during the daytime but 34 ppmv above at night (Table 2), consistent with phytoplanktonic photosynthetic activity. The different salinity ranges sampled during the daytime (0–3) and nighttime (1.4–3) do not allow accurate estimation of the NEP from diurnal variations in the upper estuary. At increasing salinities, mixing with buffered seawater creates thermodynamic conditions for CO_2 invasion and offsets some apparent heterotrophy combined with tidal advection of mangrove-derived CO_2. The latter generates a deviation (calculated as O-pCO_2 – T-pCO_2 – Ex-pCO_2) of approximately 40 ppmv of pCO_2 along the 4–25 salinity range (Fig. 6) and + 33 ppmv (daytime) and + 27 ppmv (night time) on average over the 3–34 salinity gradient (Table 2). Interestingly, our approach also suggests some autotrophic activity in the 30–33 salinity range (Fig. 6B), which is also a classical pattern of phytoplankton distribution in estuaries; indeed, blooms of marine phytoplanktonic species are a common feature in high salinity regions of river plumes, where they can benefit from the available light and nutrients and from the stratification of the water column (Cloern, 1996; Lancelot and Muylaert, 2012). Heating of water made O-pCO_2 higher than T-pCO_2 along the salinity gradient, with a maximum difference between O-pCO_2 and T-pCO_2 of +22 ppmv at salinity 32, precisely where the bloom of marine phytoplankton occurred, possibly favoured by warmer surface waters and a temporarily more stratified water column.

After conversion to CO_2 fluxes by applying a gas transfer velocity, the deviation between the T-pCO_2 and the modelled Ex-pCO_2 corrected for gas exchange provides an indirect and integrative estimate of NEP (Table 2). Quantitatively, the computed NEP (including tidal pumping) with this original method in São Francisco (Table 2), as well as in Paraiba do Sul (Cotovicz Jr. et al., 2020), is approximately 1 or less mmol m^{-2} h^{-1} when the NEP reported in estuaries of the world varies between +5 (autotrophy) and − 12 mmol m^{-2} h^{-1} (heterotrophy) (Borges and Abril, 2011). Despite these low values, our method is quite sensitive, and

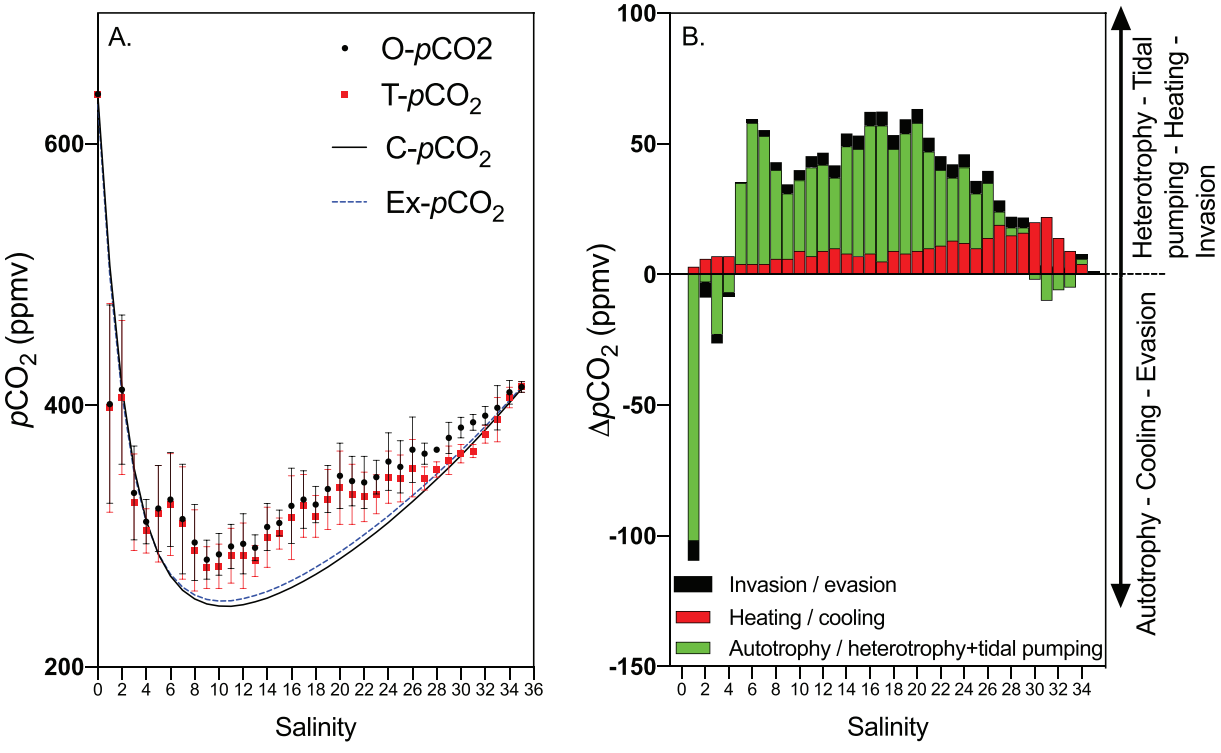

Fig. 6. Comparison between measured and modelled pCO_2 along the salinity gradient of the São Francisco Estuary during the summer and spring tide cruise in Nov. 2015. A: measured O-pCO_2 binned for one salinity increments (blue dots with standard deviations as error bars), T-pCO_2 normalized to a temperature corresponding to the conservative mixing of river and sea waters (red dots with standard deviations as error bars), modelled C-pCO_2 by considering the conservative mixing of TA, DIC and temperature in waters from the river and the sea (black full line), and modelled Ex-pCO_2 for conservative mixing corrected for gas exchange (blue dashed line). B: residual between the modelled and observed pCO_2. Invasion or evasion (black bars) is calculated as the difference between the C-pCO_2 and Ex-pCO_2 curves. Heating or cooling (red bars) is calculated as the difference between the O-pCO_2 and T-pCO_2. Autotrophy or heterotrophy and tidal pumping (green bars) is calculated as the residual, i.e. as the difference between the T-pCO_2 Ex-pCO_2. (For interpretation of the references to colour in this figure legend, the reader is referred to the web version of this article.)

Table 2
Comparison of binned data with modelled data for the Nov. 2005 campaign.

	S < 3	S < 3	S > 3	S > 3
	Day	Night	Day	Night
pCO_2 (ppmv)				
Number of measurements	518	260	701	441
Salinity range	0–2.9	1.2–3.0	3.1–35.1	3.0–30.6
Temperature	28.3 ± 0.4	27.9 ± 0.2	28.1 ± 0.4	27.7 ± 0.5
O-pCO_2	426 ± 141	421 ± 60	344 ± 39	311 ± 30
T-pCO_2	421 ± 144	420 ± 61	332 ± 37	307 ± 29
C-pCO_2	542 ± 123	392 ± 34	295 ± 46	275 ± 31
Ex-pCO_2	530 ± 123	386 ± 35	297 ± 46	277 ± 31
Components of pCO_2 deviations (ppmv)				
Heating (+)/Cooling (−)[a]	+5 ± 7	+2 ± 2	+12 ± 8	+5 ± 3
Invasion (+)/Evasion (−)[b]	−12 ± 8	−6 ± 3	+4 ± 3	+4 ± 3
Heterotrophy and tidal pumping (+)/autotrophy (−)[c]	−97 ± 77	+34 ± 19	+33 ± 25	+27 ± 17
Sum	−104 ± 90	+29 ± 21	+49 ± 39	+36 ± 22
Gas exchange parameters				
U10 (m s^{-1})	2.2 ± 1	0.4 ± 0.2	2.2 ± 1	0.4 ± 0.2
k_{600} (cm h^{-1}) W92	1.6	0.1	1.6	0.1
k_{600} (cm h^{-1}) RC01	4.1	2.2	4.1	2.2
k_{600} (cm h^{-1}) A09	7.3	2.8	7.3	2.8
CO_2 Fluxes (mmol m^{-2} h^{-1})				
Water-air CO2 flux calculated with observations	+0.47 ± 0.31	+0.15 ± 0.12	−1.00 ± 0.65	−0.61 ± 0.51
Water-air flux calculated with conservative mixing	+2.53 ± 1.65	−0.05 ± 0.05	−1.86 ± 0.51	−0.86 ± 0.72
Deviation of observations from conservative mixing	−2.06 ± 0.97	+0.20 ± 0.07	+0.86 ± 0.48	+0.25 ± 0.51
Contributions to the deviation of CO_2 fluxes (mmol m^{-2} h^{-1})				
Heating (+)/Cooling (−)	+0.10 ± 0.06	+0.01 ± 0.01	+0.20 ± 0.14	+0.10 ± 0.06
Invasion (+)/Evasion (−)	−0.21 ± 0.14	−0.04 ± 0.03	+0.03 ± 0.02	+0.01 ± 0.03
Heterotrophy plus tidal pumping (+)/autotrophy (−)	−1.94 ± 1.31	+0.23 ± 0.20	+0.62 ± 0.41	+0.14 ± 0.45

[a] Calculated as O-pCO_2 minus T-pCO_2.
[b] Calculated as C-pCO_2 minus Ex-pCO_2.
[c] Calculated as O-pCO_2 minus C-pCO_2 minus T-pCO_2 minus Ex-pCO_2. Standard deviation of the differences between two numbers were calculated as the square root of the sum of the squares of the two errors.

the sign and spatial distribution of the calculated NEP are consistent with classical concepts of estuarine plankton ecology (Crump et al., 2004; Lancelot and Muylaert, 2012), tidal advection and the short residence time in the mixing zone. This confirms the robustness of our approach, which could be applied to many estuarine environments, whether they act as CO_2 sinks or sources.

5. Conclusions

The São Francisco Estuary displays specific conditions in terms of carbonate chemistry and air-water CO_2 exchange: because of warm and poorly buffered freshwaters, oligotrophic conditions and short residence time, carbonate thermodynamic equilibration during mixing predominates over biological processes and determines water pCO_2 and air-water CO_2 fluxes. This results in an abiotic uptake of atmospheric CO_2 by the estuary at salinities above 3 in the main channel, and the DIC export to the sea is increased by 7–10%. During the winter and neap tide periods, tidal pumping and heating were weak, and the observed pCO_2 almost matched the theoretical conservative mixing curve within the error of measurements and computations. During the summer and spring tide periods, the observed pCO_2 was still below the atmospheric value but on average + 49 ppmv above the conservative mixing curve. At that season and salinities >3, heating of water relative to the mixing of the two end-members contributed to ~15%, and gas exchange contributed to ~10% of the deviation of observed pCO_2 from conservativity, the remaining ~75% being attributed in majority to tidal pumping from mangroves and brackish marshes, maybe with some respiratory activity in estuarine waters despite the short residence time. Following the approach of Cotovicz Jr. et al. (2020) in the mesotrophic and tropical Paraiba do Sul River delta, which also behaves as a CO_2 sink in the mixing zone, our study is a second detailed report of CO_2 air-water exchange based on the combination of high-resolution pCO_2 field data and theoretical computation that cover the complete salinity gradient. We highlight a singular situation, occurring not only in oligotrophic São Francisco but also in the mesotrophic Paraiba do Sul Estuary, of concomitant CO_2 uptake and heterotrophy at salinities higher than 3. Similar thermodynamic conditions, i.e., warm and poorly buffered freshwaters that potentially generate CO_2 invasion in the mixing zone, occur in large tropical river plumes such as the Amazon, Congo and Orinoco. High-resolution pCO_2 measurements along the entire salinity gradient of these large estuaries and plumes are thus necessary. In the Amazon plume, the available equilibrator pCO_2 data cover only the >17 salinity range with undersaturated values with respect to the atmosphere, well below those predicted by the conservative mixing of Amazon river water with Atlantic equatorial water (Körtzinger, 2003; Lefèvre et al., 2017). This indicates that thermodynamic and biological processes in the Amazon contribute to CO_2 invasion because the plume is autotrophic. In contrast, in the Paraiba do Sul and São Francisco Estuaries, the two processes compete with each other at both low salinities (evasion and autotrophy) and high salinities (invasion and heterotrophy). High-resolution surface pCO_2, temperature and salinity measurements coupled with modelling of estuarine mixing provided some detailed and precise information that could be applied in many plumes of large tropical rivers that contribute more significantly to the riverine carbon load to the world ocean.

Declaration of Competing Interest

None.

Acknowledgements

This research was funded by the Brazilian National Council of Research and Technological Development (CNPq) through the Science without border program (PVE 401726-6), the *Instituto do Milênio Estuários* project (420.050/2005-1) and the National Institute of Science and Technology *Transferências de Materiais Continente-Oceano* (TCMOcean 573.601/2008-9). Georgenes H Cavalcante was supported by the American University of Sharjah (research Grant FRG19-M-G74). This work is also a contribution to the International Research Project *Vulnérabilité des Ecosystèmes Littoraux Tropicaux face à l'Eutrophisation* funded by the French National Centre for Scientific Research (CNRS-INEE).

Appendix A. Supplementary data

Supplementary data to this article can be found online at https://doi.org/10.1016/j.marchem.2021.103983.

References

Abril, G., Frankignoulle, M., 2001. Nitrogen-alkalinity interactions in the highly polluted Scheldt basin (Belgium). Water Res. 35, 844–850.

Abril, G., Etcheber, H., Borges, A.V., Frankignoulle, M., 2000. Excess atmospheric carbon dioxide transported by rivers into the Scheldt estuary. C. R. Acad. Sci. Paris Série IIA 330, 761–768.
Abril, G., Etcheber, H., Delille, B., Frankignoulle, M., Borges, A.V., 2003. Carbonate dissolution in the turbid and eutrophic Loire estuary. Mar. Ecol. Prog. Ser. 259, 129–138.
Abril, G., Commarieu, M.V., Sottolichio, A., Bretel, P., Guérin, F., 2009. Turbidity limits gas exchange in a large macrotidal estuary. Estuar. Coast. Shelf Sci. 83, 342–348.
Abril, G., Bouillon, S., Darchambeau, F., Teodoru, C., Marwick, T., Tamooh, F., Ochieng Omengo, F., Geeraert, N., Deirmendjian, L., Polsenaere, P., Borges, A.V., 2015. Technical Note: Large overestimation of pCO2 calculated from pH and alkalinity in acidic, organic-rich freshwaters. Biogeosciences 12, 67–78.
Bauer, J.E., Cai, W.J., Raymond, P., Bianchi, T.S., Hopkinson, C.S., Regnier, P.G., 2013. The changing carbon cycle of the coastal ocean. Nature 504, 61–70.
Bernardes, L.M.C., 1951. Notas sobre o clima da bacia do Rio são Francisco. Rev. Bras. Geogr. 13, 473–489.
Bernardes, M.C., Knoppers, B.A., Rezende, C.E., Souza, W.F.L., Ovalle, A.R.C., 2012. Land-sea interface features of four estuaries on the South America Atlantic coast. Braz. J. Biol. 72, 761–774. https://doi.org/10.1590/S1519-69842012000400011.
Borges, A.V., 2005. Do we have enough pieces of the jigsaw to integrate CO2 fluxes in the Coastal Ocean? Estuaries 28, 3–27.
Borges, A.V., Abril, G., 2011. Carbon dioxide and methane dynamics in estuaries. In: Wolanski, E., McLusky, D.D. (Eds.), Treatise on Estuarine and Coastal Science, 5. Academic Press, Amsterdam, pp. 119–161.
Borges, A.V., Djenidi, S., Lacroix, G., Theate, J., Delille, B., Frankignoulle, M., 2003. Atmospheric CO2 flux from mangrove surrounding waters. Geophys. Res. Lett. 30, 1558.
Borges, A.V., Delille, B., Schiettecatte, L.-S., Gazeau, F., Abril, G., Frankignoulle, M., 2004. Gas transfer velocity of CO2 in three European estuaries (Randers Fjord, Scheldt and Thames). Limnol. Oceanogr. 49, 1630–1641.
Borges, A.V., Schiettecatte, L.-S., Abril, G., Delille, B., Gazeau, F., 2006. Carbon dioxide in European coastal waters. Estuar. Coast. Shelf Sci. 70, 375–387.
Bouillon, S., Frankignoulle, M., Dehairs, F., Velimirov, B., Eiler, A., Abril, G., Etcheber, H., Borges, A.V., 2003. Inorganic and organic carbon biogeochemistry in the Gautami Godavari estuary (Andhra Pradesh, India) during pre-monsoon: the local impact of extensive mangrove forests. Glob. Biogeochem. Cy. 17, 1114.
Cai, W.J., 2011. Estuarine and coastal ocean carbon paradox: CO2 sinks or sites of terrestrial carbon incineration? Annu. Rev. Mar. Sci. 3, 123–145.
Cai, W.J., Wang, Y., Hodson, R.E., 1998. Acid-Base Properties of Dissolved Organic Matter in the Estuarine Waters of Georgia, USA. Geochimica et Cosmochimica Acta 62 (3), 473–483.
Cai, W.J., Chen, A.C., Borges, A.V., 2013. Carbon dioxide dynamics and fluxes in coastal waters influenced by river plumes. In: Bianchi, T., Allison, M., Cai, W. (Eds.), Biogeochemical Dynamics at Major River-Coastal Interfaces: Linkages with Global Change. Cambridge University Press, pp. 155–173. https://doi.org/10.1017/CBO9781139136853.010.
Cavalcante, G., Miranda, L.B., Medeiros, P.R.P., 2017. Circulation and salt balance in the São Francisco river Estuary (NE/Brazil). Rev. Bras. Recur. Hidr. 22 https://doi.org/10.1590/2318-0331.021720170003.
Cavalcante, G., Vieira, F., Campos, E., Brandini, N., Medeiros, P.R.P., 2020. Temporal streamflow reduction and impact on the salt dynamics of the São Francisco River Estuary and adjacent coastal zone (NE/Brazil). Reg. Stud. Mar. Sci. 38, 101363. https://doi.org/10.1016/j.rsma.2020.101363.
Chen, C.T.A., Borges, A.V., 2009. Reconciling opposing views on carbon cycling in the coastal ocean: continental shelves as sinks and near-shore ecosystems as sources of atmospheric CO_2. Deep Sea Res. Part 2 Top. Stud. Oceanogr. 56, 578–590.
Chen, C.T.A., Huang, T.-H., Fu, Y.-H., Bai, Y., He, X., 2012. Strong sources of CO2 in upper estuaries become sinks of CO2 in large river plumes. Curr. Opin. Environ. Sustain. 4, 179–185. https://doi.org/10.1016/j.cosust.2012.02.003.
Cloern, J.E., 1996. Phytoplankton bloom dynamics in coastal ecosystem: a review with some general lessons from sustained investigation of San Francisco Bay, California. Rev. Geophys. 34, 127–168.
Cotovicz Jr., L.C., Knoppers, B.A., Brandini, N., Costa Santos, S.J., Abril, G., 2015. A strong CO2 sink enhanced by eutrophication in a tropical coastal embayment (Guanabara Bay, Rio de Janeiro, Brazil). Biogeosciences 12, 6125–6146.
Cotovicz Jr., L.C., Libardoni, B., Brandini, N., Knoppers, B., Abril, G., 2016. Comparações entre medições em tempo real da pCO2 aquática com estimativas indiretas em dois estuárioss tropicais contrastantes: o estuário eutrofizado da Baia de Guanabara (RJ) e o estuário oligotrofico do Rio São Francisco (AL). Quím. Nova 39, 1206–1214.
Cotovicz Jr., L.C., Vidal, L.O., de Rezende, C.E., Bernardes, M.C., Knoppers, B.A., Sobrinho, R.L., Cardoso, R.P., Muniz, M., dos Anjos, R.M., Biehler, A., Abril, G., 2020. Carbon dioxide sources and sinks in the delta of the Paraíba do Sul River (Southeastern Brazil) modulated by carbonate thermodynamics, gas exchange and ecosystem metabolism during estuarine mixing. Mar. Chem. 226 (20), 103869.
Cotovicz Jr., L.C., Ribeiro, R., Régis, C.R., Bernardes, M., Sobrinho, R., Vidal, L.O., Tremmel, D., Knoppers, B.A., Abril, G., 2021. Greenhouse gas emissions (CO_2 and CH_4) and inorganic carbon behavior in an urban highly polluted tropical coastal lagoon (SE, Brazil). Environ. Sci. Pollut. Res. https://doi.org/10.1007/s11356-021-13362-2.
Crump, B.C., Hopkinson, C.S., Sogin, M.L., Hobbie, J.E., 2004. Microbial biogeography along an estuarine salinity gradient: combined influences of bacterial growth and residence time. Appl. Environ. Microbiol. 70, 1494–1505.2.
de Jong, P., Tanajura, C.A.S., Sánchez, A.S., Dargaville, R., Kiperstok, A., Torres, E.A., 2018. Hydroelectric production from Brazil's São Francisco River could cease due to climate change and inter-annual variability. Sci. Total Environ. 634, 1540–1553.
Delaigue, L., Thomas, H., Mucci, A., 2020. Spatial variations in CO2 fluxes in the Saguenay Fjord (Quebec, Canada) and results of a water mixing model. Biogeosciences 17, 547–566. https://doi.org/10.5194/bg-17-547-2020.
Dickson, A.G., Millero, F.J., 1987. A comparison of the equilibrium constants for the dissociation of carbonic acid in seawater media. Deep-Sea Res. 34, 1733–1743.
Dinauer, A., Mucci, A., 2017. Spatial variability in surface-water pCO2 and gas exchange in the world's largest semi-enclosed estuarine system: St. Lawrence estuary (Canada). Biogeosciences 14, 3221–3237.
Dominguez, J.M.L., 1996. The São Francisco strandplain: a paradigm for wave-dominated deltas? Geol. Soc. Lond. Spec. Publ. 117, 217–231.
Etemad-Shahidi, A., Imberger, J., 2002. Anatomy of turbulence in a narrow and strongly stratified estuary. J. Geophys. Res. 107, 3070. https://doi.org/10.1029/2001JC000977.
Frankignoulle, M., Bourge, I., Wollast, R., 1996. Atmospheric CO2 fluxes in a highly polluted estuary (the Scheldt). Limnol. Oceanogr. 41, 365–369.
Frankignoulle, M., Abril, G., Borges, A., Bourge, I., Canon, C., Delille, B., Libert, E., Théate, J.M., 1998. Carbon dioxide emission from European estuaries. Science 282, 434–436.
Frankignoulle, M., Borges, A.V., Biondo, R., 2001. A new design of equilibrator to monitor carbon dioxide in highly dynamic and turbid environments. Water Res. 35, 1344–1347.
Grodsky, S.A., Reverdin, G., Carton, J.A., Coles, V.J., 2014. Year-to-year salinity changes in the Amazon plume: contrasting 2011 and 2012 Aquarius/SACD and SMOS satellite data. Remote Sens. Environ. 140, 14–22.
Hunt, C.W., Salisbury, J.E., Vandemark, D., 2011. Contribution of non-carbonate anions to total alkalinity and overestimation of pCO2 in New England and New Brunswick rivers. Biogeosciences 8, 3069–3076.
Körtzinger, A., 2003. A significant CO_2 sink in the tropical Atlantic Ocean associated with the Amazon river plume. Geophys. Res. Lett. 30, 2287. https://doi.org/10.1029/2003GL018841.
Lancelot, C., Muylaert, K., 2012. Trends in Estuarine Phytoplankton Ecology. In: Wolanski, E., McLusky, D.D. (Eds.), Treatise on Estuarine and Coastal Science, 7. Academic Press, Amsterdam, pp. 5–15.
Lefèvre, N., Flores, Montes M., Gaspar, F.L., Rocha, C., Jiang, S., De Araújo, M.C., Ibánhez, J.S.P., 2017. Net heterotrophy in the Amazon continental shelf changes rapidly to a sink of CO_2 in the outer amazon plume. Front. Mar. Sci. 4, 278. https://doi.org/10.3389/fmars.2017.00278.
Leopold, A., Marchand, C., Deborde, J., Allenbach, M., 2016. Water biogeochemistry of a mangrove-dominated estuary under a semi-arid climate (New Caledonia). Estuar. Coasts 40, 773–791.
Maher, D.T., Santos, I.R., Golsby-Smith, L., Gleeson, J., Eyre, B.D., 2013. Groundwater-derived dissolved inorganic and organic carbon exports from a mangrove tidal creek: the missing mangrove carbon sink? Limnol. Oceanogr. 58, 475–488.
Maher, D.T., Call, M., Santos, I.R., Sanders, C., 2018. Beyond burial: lateral exchange is a significant atmospheric carbon sink in mangrove forests. Biol. Lett. 14 https://doi.org/10.1098/rsbl.2018.0200.
Medeiros, P.P.M., Knoppers, B.A., Cavalcante, G.H., de Souza, W.F.L., 2011. Changes in nutrient loads (N, P and Si) in the São Francisco estuary after the construction of dams. Braz. Arch. Biol. Technol. 54, 387–397.
Medeiros, P.R.P., Knoppers, B.A., dos Santos, Júnior R.C., de Souza, W.F.L., 2007. Aporte fluvial e dispersão de matéria particulada em suspensão na zona costeira do Rio São Francisco (SE/AL). Geochim. Bras. 21 (2), 212–231.
Medeiros, P.R.P., Cavalcante, G.H., Melo, E.R., Brandini, N., 2018. The são Francisco river (NE): review on the interannual loading of particulate matter suspended to the ocean and impacts of dams. Int. J. Hydrol. 2, 190–193. https://doi.org/10.15406/ijh.2018.02.00067.
Mehrbach, C., Culberson, C.H., Hawley, J.E., Pytkowicz, R.M., 1973. Measurements of the apparent dissociation constants of carbonic acid in seawater at atmospheric pressure. Limnol. Oceanogr. 18, 897–907.
Melo, E.R., Brandini, N., Medeiros, P.R.P., Silva, R., Cavalcante, G., 2020. Nutrients load estimation in a regulated Streamflow estuary: the São Francisco estuary (NE/Brazil). Rev. Bras. Meteorol. 35, 803–811.
Melo-Magalhães, E.M., Moura, A.N., Medeiros, P.R.P., Koening, M.L., 2015. Microphytoplankton biomass and trophic state of the estuarine region of the São Francisco River (Northeastern Brazil) *Braz.* J. Aquat. Sci. Technol. 20, 19–30.
Murgulet, D., Trevino, M., Douglas, A., Spalt, N., Hu, X., Murgulet, V., 2018. Temporal and spatial fluctuations of groundwater-derived alkalinity fluxes to a semiarid coastal embayment. Sci. Total Environ. 630, 1343–1359. https://doi.org/10.1016/j.scitotenv.2018.02.333.
Neubauer, S.C., Anderson, I.C., 2003. Transport of dissolved inorganic carbon from a tidal freshwater marsh to the York River estuary. Limnol. Oceanogr. 48, 299–307.
Orton, P.M., Zappa, C.J., McGillins, W.R., 2010. Tidal and atmospheric influences on near-surface turbulence in an estuary. J. Geophys. Res. 115, C12029 https://doi.org/10.1029/2010JC006312.
Phillipson, L., Toumi, R., 2020. Assimilation of satellite salinity for modelling the Congo River plume. Remote Sens. 12, 11. https://doi.org/10.3390/rs12010011.
Pierrot, D., Lewis, D.E., Wallace, D.W.R., 2006. MS Excel Program Developed for CO2 System Calculations. ORNL/CDIAC-105a. Carbon Dioxide Information Analysis Center, Oak Ridge National Laboratory, U.S. Department of Energy, Oak Ridge, Tennessee. https://doi.org/10.3334/CDIAC/otg.CO2SYS_XLS_CDIAC105a.
Raymond, P.A., Cole, J.J., 2001. Gas exchange in rivers and estuaries: choosing a gas transfer velocity. Estuaries 24, 312–317.
Santos, I.R., Maher, D.T., Larkin, R., Webb, J., Sanders, C.J., 2018. Carbon outwelling and outgassing vs. burial in an estuarine tidal creek surrounded by mangrove and saltmarsh wetlands. Limnol. Oceangr. Letters 2, 1–18. https://doi.org/10.1002/lno.11090.

Sarma, V., Viswanadham, R., Rao, G.D., Prasad, V.R., Kumar, B.S.K., Naidu, S.A., Kumar, N.A., Rao, D.B., Sridevi, T., Krishna, M.S., Reddy, N.P.C., Sadhuram, Y., Murty, T.V.R., 2012. Carbon dioxide emissions from Indian monsoonal estuaries. Geophys. Res. Lett. 39, L03602 https://doi.org/10.1029/2011gl050709.

Smith, S.V., Hollibaugh, J.T., 1993. Coastal metabolism and the oceanic carbon balance. Rev. Geophys. 31, 75–89.

Strickland, J.D.H., Parsons, T.R., 2010. A practical handbook of seawater analysis, 2nd edn. Fisheries Research Board of Canada Bulletin, Ottawa, Canada.

Takahashi, T., Sutherland, S.C., Sweeney, C., Poisson, A., Metzl, N., Tilbrook, B., Bates, N., Wanninkhof, R., Feely, R.A., Sabine, C., Olafsson, J., Nojiri, Y., 2002. Global sea-air CO2 flux based on climatological surface ocean pCO2, and seasonal biological and temperature effects. Deep-Sea Res. II Top. Stud. Oceanogr. 49, 1601–1622.

Wanninkhof, R., 1992. Relationship between wind speed and gas exchange over the ocean. J. Geophys. Res. 97, 7373–7382.

Weiss, R.F., 1974. Carbon dioxide in water and seawater: the solubility of a non-ideal gas. Mar. Chem. 2, 203–215.

Whitfield, M., Turner, D.R., 1986. The carbon dioxide system in estuaries – an inorganic perspective. Sci. Total Environ. 49, 235–255.

Wollast, R., 1991. The coastal organic carbon cycle: Fluxes, sources, and sinks. In: Mantoura, R.F.C., Martin, J.M., Wollast, R. (Eds.), Ocean Margin Processes in Global Change. Wiley, Chichester, West Sussex, England, pp. 365–381.

Yao, H., Hu, X., 2017. Responses of carbonate system and CO_2 flux to extended drought and intense flooding in a semiarid subtropical estuary. Limnol. Oceanogr. 62, S112–S130.

Yao, H., McCutcheon, M.R., Staryk, C.J., Hu, X., 2020. Hydrologic controls on CO_2 chemistry and flux in subtropical lagoonal estuaries of the northwestern Gulf of Mexico. Limnol. Oceanogr. 9999 (2020), 1–19. https://doi.org/10.1002/lno.11394.